

Turbulent thermal convection across a stable liquid-liquid interface

Hailong Huang ^{1,2} Yin Wang ^{2,*} Wei Xu ² Xiaozhou He,^{1,†} and Penger Tong ^{2,3,‡}

¹*School of Mechanical Engineering and Automation, Harbin Institute of Technology, Shenzhen, China*

²*Department of Physics, Hong Kong University of Science and Technology,
Clear Water Bay, Kowloon, Hong Kong*

³*Center for Ocean Research in Hong Kong and Macau, Hong Kong University of Science and Technology,
Clear Water Bay, Kowloon, Hong Kong*



(Received 1 January 2024; accepted 29 February 2024; published 22 March 2024)

We report a systematic study of turbulent thermal convection across two vertically stacked layers of immiscible fluids, FC770 and water, with a stable liquid-liquid interface even when each fluid layer is under turbulent convection. The normalized mean temperature profile $\theta(z)$ and temperature variance profile $\Omega(z)$, as a function of distance z away from the interface, are measured along the central vertical axis of the cylindrical convection cell with varying temperature difference Δ across the cell. From the measured mean temperature and temperature variance profiles, we find a unique twin-boundary-layer structure across the liquid interface with one of the twin boundary layers (BLs) residing on each side of the interface. The measured $\theta(z)$ and $\Omega(z)$ in each fluid layer are found to have the scaling forms $\theta(z/\lambda)$ and $\Omega(z/\lambda)$, respectively, with varying BL thickness λ , and their functional forms are well described by the equations for a BL attaching to a solid conducting plate, so long as a thermal slip length ℓ_T is introduced to account for the convective heat flux passing through the liquid interface. While the obtained $\theta(z/\lambda)$ and $\Omega(z/\lambda)$ for the twin BLs share the same scaling forms, they nevertheless have different BL thickness λ and slip length ℓ_T in the two fluid layers. Furthermore, three characteristic temperatures are found as response parameters in the two-layer convection, namely, the mean temperature T_0 of the interface, the mean bulk temperature T_F of the FC770 layer, and the mean bulk temperature T_W of the water layer. By combining the scaling result of heat transport across the entire cell and the effects of broken symmetry between the BL near the conducting plate and that near the liquid interface, we obtain three quantitative relations that link the three characteristic temperatures to the normalized slip length $\xi_0 = (1 + \lambda/\ell_T)^{-1}$ and the temperature difference Δ . The theoretical predictions are found in good agreement with the experimental results.

DOI: [10.1103/PhysRevFluids.9.033502](https://doi.org/10.1103/PhysRevFluids.9.033502)

I. INTRODUCTION

As a classical model system, Rayleigh-Bénard convection (RBC) has been used for the study of a range of hydrodynamic problems over a hundred years. In the laboratory, RBC is realized in a single fluid layer confined between two horizontally parallel conducting plates, which are heated from below and cooled from the top with a vertical temperature difference ΔT parallel to gravity. When the Rayleigh number (dimensionless buoyancy proportional to ΔT) is sufficiently large (e.g.,

*Now at Princeton Plasma Physics Laboratory, Princeton University, Princeton, NJ 08543, USA.

†hexiaozhou@hit.edu.cn

‡penger@ust.hk

$Ra \gtrsim 10^8$), the bulk fluid becomes turbulent and a large-scale circulation (LSC) is formed across the convection cell [1,2]. The LSC is driven by the warm and cold plumes emitted from the unstable thermal boundary layers (BLs) near the bottom and top conducting plates [3–6] and is maintained in a turbulent environment. Turbulent RBC has been studied extensively in the upright cylindrical cells of radius-to-height aspect ratio unity, in which the LSC has a single roll structure with its size comparable to the cell height H [7–10]. As a wall-bounded flow, turbulent RBC has temperature and velocity BLs adjacent to the conducting plates, and their dynamics are of great importance, as the thermal BLs determine the global heat transport of the system [11,12].

In addition to the large number of investigations on thermal convection in a single fluid layer, theoretical and experimental efforts have also been made to study thermal convection in two-layer systems consisting of two stacking layers of immiscible fluids with a stable liquid interface. Early studies of two-layer convection [13–17] focused mainly on the laminar region, in which the liquid interface is considered to be stationary and heat transport across the interface is made only by thermal conduction. In this case, the temperature at the liquid interface can be derived directly from the conservation requirement of heat flux across the entire system. In recent years, the studies of two-layer convection have expanded into the turbulence regime [18–22], in which the convective flow in each fluid layer was found to be turbulent and possess the key features of single-layer turbulent convection [5,6,23,24]. Due to the coupling of the large-scale flows between the two immiscible fluid layers [18–20], the liquid interface undergoes strong fluctuations with a net convective heat flux passing through it. Nonetheless, the liquid interface is still stable and remains in an average position with minimal movement.

In a more recent study [25], Huang *et al.* reported the measurements of thermal BL profiles across a stable and immiscible liquid-liquid (water-FC770) interface formed in two-layer turbulent Rayleigh-Bénard convection. Understanding the BL flow near a liquid interface is relevant to a number of important natural phenomena, such as the coupled ocean-atmosphere flows [26] and convection of the Earth’s upper and lower mantles [27,28], and many industrial applications ranging from the liquid-encapsulated crystal growth technique [29] to solvent extraction [30]. Airflow through the respiratory system [31] is another example of two-layer flow, which involves complex flow patterns and transport processes along the airway passages that are important for the physiological processes related to breathing and gas exchange. A central finding of the investigation by Huang *et al.* is that the measured mean temperature and temperature variance profiles near the liquid interface can all be well described by the BL equations for a solid wall, so long as a thermal slip length ℓ_T is included to account for the convective heat flux passing through the liquid interface.

On a solid conducting plate, the no-slip and no-fluctuation boundary conditions dictate that

$$\langle w'T' \rangle_t = 0, \quad \partial_z \langle w'T' \rangle_t = 0, \quad \partial_z^2 \langle w'T' \rangle_t = 0, \quad (1)$$

where $\langle w'T' \rangle_t$ is the velocity-temperature correlation function with T' and w' being, respectively, the local temperature and vertical velocity fluctuations, and $\langle \dots \rangle_t$ denotes an average over time t . In this case, Shishkina *et al.* [4] introduced the turbulent thermal diffusivity $\kappa_t(z)$ to describe the convective heat transfer, $\langle w'T' \rangle_t = -\kappa_t(z)\partial_z \langle T \rangle_t$, and showed that near a solid wall, $\kappa_t(z)$ has a scaling form, $[\kappa_t(z)]_S \simeq a\kappa\xi_S^3$, in the leading order, where a is a proportionality constant, κ is the molecular thermal diffusivity of the convecting fluid, and $\xi_S = z/\lambda_S$ is the vertical distance z away from the solid surface normalized by the thermal BL thickness λ_S . Hereafter, we use the subscripts S and L to indicate the quantities that are obtained near a solid conducting plate and a liquid interface, respectively.

At a stable liquid interface, however, while the mean vertical velocity is zero, the local temperature and vertical velocity fluctuations are nonzero, i.e., $T' \neq 0$ and $w' \neq 0$, and consequently one has [25]

$$\langle w'T' \rangle_t \neq 0, \quad \partial_z \langle w'T' \rangle_t \neq 0, \quad \partial_z^2 \langle w'T' \rangle_t \neq 0. \quad (2)$$

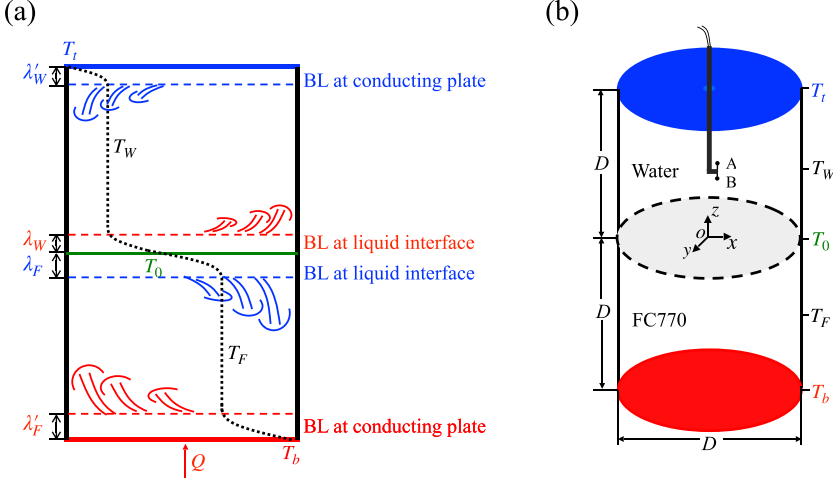


FIG. 1. (a) Sketch of the two-layer convection system. The black dotted line indicates a typical mean temperature profile across the cell height. The temperature of the top conducting plate ($z = D$) is T_t and that of the bottom conducting plate ($z = -D$) is T_b . The temperature of the liquid interface ($z = 0$) is T_0 . The bulk fluid temperature of the FC770 layer is T_F and that of the water layer is T_W . The thickness of the two BLs in the FC770 layer is denoted as λ'_F (near the liquid interface) and λ'_W (near the conducting plate), respectively. Similarly, the thickness of the two thermal BLs in the water layer is denoted as λ'_W (near the liquid interface) and λ'_W (near the conducting plate), respectively. (b) Sketch of the experimental set-up for the measurement of local temperature profiles along the central vertical axis of the convection cell. The inner diameter of the upright cylinder is $D = 190$ mm and its height is $H = 2D$. Also shown is the coordinate system used in the experiment.

In this case, $\kappa_t(z)$ will contain all lower-order terms in general. Huang *et al.* demonstrated both by experiment and direct numerical simulation (DNS) [25] that the turbulent thermal diffusivity near a liquid interface has a complete cubic form, $[\kappa_t(\xi)]_L \simeq a\kappa(\xi_L + \xi_0)^3$, where $\xi_0 \equiv \ell_T/\lambda_S \simeq \ell_T/(\lambda_L + \ell_T)$ is the normalized slip length. In the study of BL profiles, one often uses the normalized mean temperature profile $\theta_L(z) = |\langle T(z, t) \rangle_t - \langle T(z = 0, t) \rangle_t|/\Delta T$, where z is the vertical distance away from the liquid interface and ΔT is the temperature difference across the BL. It was found that the measured $\theta_L(\xi_L)$ near the liquid interface has the scaling form [25],

$$\theta_L(\xi_L; c, \xi_0) = \frac{1}{b} \int_{\xi_0}^{b\xi_L + \xi_0} (1 + a\epsilon^3)^{-c} d\epsilon, \quad (3)$$

where $\xi_L = z/\lambda_L$ is the vertical distance z away from the liquid interface normalized by the thermal BL thickness λ_L , and $b \simeq 1 - \xi_0$ is used to re-normalize the slip-induced local slope change of the temperature profile. It can also be viewed as a correction of the BL thickness. The parameter $c (\geq 1)$ in Eq. (3) satisfies the condition $a = [\Gamma(1/3)\Gamma(c - 1/3)/3\Gamma(c)]$ [4].

When the normalized slip length $\xi_0 = 0$, Eq. (3) reduces to an equation for the normalized mean temperature profile $\theta_S(\xi_S; c)$ near a conducting plate [4]

$$\theta_S(\xi_S; c) = \int_0^{\xi_S} (1 + a\epsilon^3)^{-c} d\epsilon. \quad (4)$$

Equation (4) has only one fitting parameter c . When $c \rightarrow \infty$, $\theta_S(\xi_S; \infty)$ approaches the Prandtl-Blasius-Pohlhausen (PBP) form [32] for a laminar BL without any fluctuations. If the value of c can be obtained from the conducting plate, then the number of fitting parameters in Eq. (3) is reduced to one, i.e., ξ_0 . Figure 1(a) shows a sketch of a typical mean temperature profile in turbulent convection across the two fluid layers.

Another important quantity to characterize BL fluctuations is the normalized temperature variance profile, $\Omega_L(\xi_L) \equiv (\eta(\xi_L)/\eta_p)_L$, where $\eta_L(z) = \langle [T(z, t) - \langle T(z, t) \rangle_t]^2 \rangle_t$ is the temperature variance and η_p is its peak value located at the outer edge of the BL. For a laminar BL without any fluctuations, one has $\Omega_L(\xi_L) = 0$. The measured $\Omega_L(\xi_L)$ near the liquid interface was found to have the scaling form [25],

$$\Omega_L(\xi_L; c, \xi_0) = \Omega_S(b\xi_L + \xi_0; c), \quad (5)$$

where $\Omega_S(\xi_S) = (\eta(\xi_S)/\eta_p)_S$ is the normalized temperature variance profile near a solid conducting plate, which can be solved numerically from the ordinary differential equation [5,37],

$$\begin{aligned} (1 + d\xi_S^3) \frac{d^2\Omega_S(\xi_S)}{d\xi_S^2} + (\tau + 3d)\xi_S^2 \frac{d\Omega_S(\xi_S)}{d\xi_S} + 2 \frac{\Delta_b^2}{\eta_p} \frac{a\xi_S^3}{(1 + a\xi_S)^{2c}} - \frac{1}{2} \frac{[d\Omega_S(\xi_S)/d\xi_S]^2}{\Omega_S(\xi_S)} \\ - 2\alpha\Omega_S(\xi_S) = 0. \end{aligned} \quad (6)$$

In the recent work by Huang *et al.* [25], the above theoretical framework was tested only in one of the two fluid layers, which were confined in a quasi-two-dimensional (quasi-2D) thin disk with its stadium-shaped cross-section in parallel with gravity. In this work, we extend our investigation to further test the universality of the BL properties across the liquid interface. In particular, we use an upright cylinder of aspect ratio 0.5 as the convection cell, which allows more 3D flow modes in each fluid layer [33–36]. The mean temperature and temperature variance profiles are measured both above and below the liquid interface so that a comparative study of the BL properties is conducted between the twin BLs across the liquid interface. The obtained mean temperature profile $\theta_L(z)$ and temperature variance profile $\Omega_L(z)$ for the twin BLs are found to share the same scaling forms, but they have different BL thickness λ_L and slip length ℓ_T in the two fluid layers. Furthermore, we obtain three quantitative relations that link the three characteristic temperatures of the two-layer convection to the normalized slip length ξ_0 and the temperature difference Δ across the entire cell. The theoretical analysis is found to be in good agreement with the experimental results.

The remainder of the paper is organized as follows. We first describe the experimental methods in Sec. II. Experimental results are presented in Sec. III. Finally, the work is summarized in Sec. IV.

II. EXPERIMENT

As illustrated in Fig. 1(b), the two-layer convection cell is an upright cylinder with an inner diameter $D = 19.0$ cm and a height $H = 2D = 38.0$ cm. The corresponding aspect ratio of the cell is $\Gamma \equiv D/H = 0.5$. The convection cell is similar to those used in the previous experiments [37–39] and here we only mention some key features. The sidewall of the cell is made of a transparent Plexiglas ring with a wall thickness of 0.6 cm. The top and bottom plates are made of 1-cm-thick brass plates and their surfaces are electroplated with a thin layer of gold. Two silicon rubber film heaters (Omega, SRFR 7/10) connected in parallel are sandwiched on the backside of the bottom plate to provide constant and uniform heating. The top plate is cooled by a closed cooling chamber, in which cooling water is regulated by a temperature-controlled chiller (NESLAB, RTE740) with a temperature stability of 10 mK. Three thermistors with an accuracy of 5 mK are embedded in each brass plate 1 mm away from the conducting surface to record the bottom temperature (T_b) and top temperature (T_t). The temperature difference, $\Delta = T_b - T_t$, across the cell is thus measured and varied from 4.9 to 47.7°C by changing the heating power. The lower half of the cell is filled with a fluorinated liquid, FC770 (3M Fluorinert FC770), and the upper half of the cell is filled with distilled water, which is immiscible with FC770 and has a lower density. Therefore, the aspect ratio of each fluid layer is unity.

The dimensionless control parameters for the two-layer system are the Rayleigh number defined as $\text{Ra}_i = \beta_i g D^3 \Delta_i / (\nu_i \kappa_i)$ and the Prandtl number defined as $\text{Pr}_i = \nu_i / \kappa_i$, where the subscript i indicates the two different fluid layers with $i = F$ for FC770 and $i = W$ for water, g is the gravitational acceleration, and Δ_i is the temperature difference across the i -th fluid layer of height D . The values

TABLE I. Two liquid samples used in the experiment and their literature values of density ρ , dynamic viscosity μ , thermal diffusivity κ , thermal conductivity k , thermal expansion coefficient β , and surface tension with air γ at specified temperatures T . The properties of water and FC770 are obtained, respectively, from Refs. [40] and [41].

Fluids	T (°C)	ρ (g/cm ³)	μ (mPa s)	κ (mm ² /s)	k [W/(m K)]	β (1/mK)	γ (mN/m)	Pr
FC770	40.00	1.755	1.140	0.039	0.099	1.48	~14.8	20.0
	19.20	0.998	1.021	0.143	0.598	0.177	72.53	7.30
Water	29.74	0.996	0.809	0.149	0.618	0.317	71.03	5.43
	34.52	0.994	0.733	0.151	0.626	0.349	70.28	4.86
	37.99	0.993	0.685	0.152	0.632	0.372	69.74	4.30

of the thermal expansion coefficient β_i , kinematic viscosity ν_i , and thermal diffusivity κ_i of each fluid at specified temperatures are given in Table I. Another important dimensionless parameter is the Weber number defined as $We = \rho_F \beta_F \Delta g H^2 / \gamma'$ with γ' being the interfacial tension of the FC770-water interface [25]. The Weber number measures the relative importance of the inertial forces compared to the surface tension forces. In this work, we focus on the two thermal BLs near the interface; one is beneath the liquid interface in the FC770 layer and the other is above the liquid interface in the water layer. By adjusting the temperature of the cooling water, the bulk temperature (T_F) of the FC770 layer is maintained at $40 \pm 0.05^\circ\text{C}$ with a fixed Prandtl number $Pr_F = 20.0$ for all the measurements. The bulk temperature (T_W) of the water layer is varied from 19.2 to 37.0°C with $4.3 \lesssim Pr_W \lesssim 7.3$. In the experiment, we vary the total temperature difference, $\Delta = \Delta_F + \Delta_W$, across the cell, so that the resulting Ra_F is varied in the range $2.1 \times 10^{10} \lesssim Ra_F \lesssim 1.8 \times 10^{11}$, Ra_W is in the range $2.3 \times 10^8 \lesssim Ra_W \lesssim 1.2 \times 10^9$, and We is in the range $25 \lesssim We \lesssim 250$, as shown in Table II.

Two identical waterproof thermistors (AB6E3-B05KA202R, Thermometrics) are used to measure the local temperature of the convecting fluid. The two thermistors have a diameter of 0.17 mm with a response time of 10 ms. They are assembled, with one bead pointing upward and the other bead pointing downward, as illustrated in Fig. 1(b). To guide the thermistors and their connecting wires into the convection cell, a thin stainless steel tube with a diameter of 1.2 mm is installed through the center of the cooling chamber. The stainless steel tube is mounted on a translation stage, which is controlled by a stepping motor for precise positioning of the thermistors at different locations across the liquid interface. To minimize the wetting effect of the liquid interface on the thermistor, we measure the local temperature profiles $T(z, t)$ above and below the liquid interface separately. Thermistor B is used to measure $T(z, t)$ above the interface when the probe is moving downward (advancing direction) from above the liquid interface. Thermistor A is used to measure $T(z, t)$ below the interface when the probe is moving upward (receding direction) from below the liquid interface. The whole temperature profile $T(z, t)$ is then obtained by combining the two parts of $T(z, t)$, and the exact position of the liquid interface is determined by extrapolation. This is a

TABLE II. Experimental parameters obtained from different experimental runs.

Run	T_b (°C)	T_t (°C)	T_F (°C)	T_W (°C)	T_0 (°C)	λ_F (mm)	λ_W (mm)	Ra_F	Ra_W	We
1	58.87	11.17	40.05	19.20	23.81	0.98	1.13	1.8×10^{11}	1.2×10^9	250
2	50.07	25.87	39.97	29.74	31.70	1.12	1.20	9.5×10^{10}	9.8×10^8	131
3	45.22	32.61	40.03	34.52	35.58	1.19	1.39	5.0×10^{10}	6.2×10^8	69
4	42.25	37.35	40.00	37.99	38.39	1.23	1.54	2.1×10^{10}	2.3×10^8	25

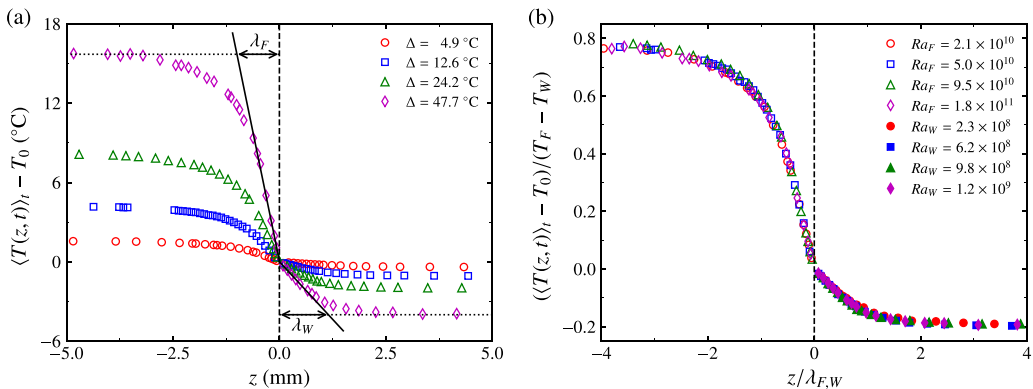


FIG. 2. (a) Measured mean temperature profiles $\langle T(z, t) \rangle_t$ (colored symbols) as a function of distance z away from the liquid interface for different temperature differences Δ across the convection cell. In the plot, the temperature T_0 at the liquid interface is used as a temperature reference point and thus is subtracted from the mean temperature profiles. The solid lines indicate the local slope of the measured $\langle T(z, t) \rangle_t$ on each side of the liquid interface at $\Delta = 47.7^\circ\text{C}$. The resulting thermal BL thickness on the FC770 side is $\lambda_F = 0.98$ mm and that on the water side is $\lambda_W = 1.13$ mm. (b) Normalized mean temperature profiles $(\langle T(z, t) \rangle_t - T_0) / (T_F - T_W)$ as a function of the normalized distance $z / \lambda_{F,W}$ for different Rayleigh numbers. For $z < 0$ (FC770 layer), z is normalized by the BL thickness λ_F in the FC770 layer. For $z > 0$ (water layer), z is normalized by the BL thickness λ_W in the water layer. Here, $T_F - T_W$ is the temperature difference between the two bulk fluids.

new procedure, which was not used in the previous work (see, e.g., Fig. 4 in Ref. [25]). With this procedure, we correct the slight offset that the interface experiences when the thermistor crosses it.

The entire cell is wrapped with Styrofoam and placed inside a thermostat box, to minimize heat exchange between the convecting fluid and the surroundings. The temperature of the thermostat box is set to match the mean temperature of the bulk FC770 fluid ($40 \pm 0.05^\circ\text{C}$). More details about the high-precision temperature measurements across the liquid interface have been described elsewhere [25]. This experimental setup ensures an accurate measurement of $T(z)$ and minimizes the external influences on the temperature field of the convecting fluid.

III. EXPERIMENTAL RESULTS

A. Scaling behavior of the measured mean temperature and temperature variance profiles

Figure 2(a) shows the measured mean temperature profiles, $\langle T(z, t) \rangle_t - T_0$, as a function of distance z away from the liquid interface for different temperature differences Δ across the convection cell. The mean temperature $\langle T(z, t) \rangle_t$ is obtained from the time series data $T(z, t)$ obtained at different locations z . The temperature T_0 at the interface is used as a temperature reference point and is determined by a linear extrapolation of the local slope (black solid lines) of the measured $\langle T(z, t) \rangle_t$ on both sides of the liquid interface. In this way, all the mean temperature profiles pass through the zero point at the interface. It is seen that the measured $\langle T(z, t) \rangle_t - T_0$ changes linearly with distance z when the absolute value of z is small (i.e., for positions very close to the interface) and gradually approaches a constant value when z is moved far away from the interface. The asymptotic values of $\langle T(z, t) \rangle_t$ are the bulk fluid temperatures T_F for the FC770 layer with $z < 0$ and T_W for the water layer with $z > 0$. The three characteristic temperatures of the two-layer system, namely T_0 , T_F and T_W , all change with the temperature difference Δ across the convection cell. It is found that the measured mean temperature $\langle T(z, t) \rangle_t$ across the interface is continuous and does not have a jump, whereas the measured temperature gradient $d\langle T(z, t) \rangle_t / dz$ has a finite jump at the interface with the measured values of $d\langle T(z, t) \rangle_t / dz$ below the interface being much larger than that above the interface, as indicated by the two solid lines with a slope of -16.50 K/mm on the FC770 side and

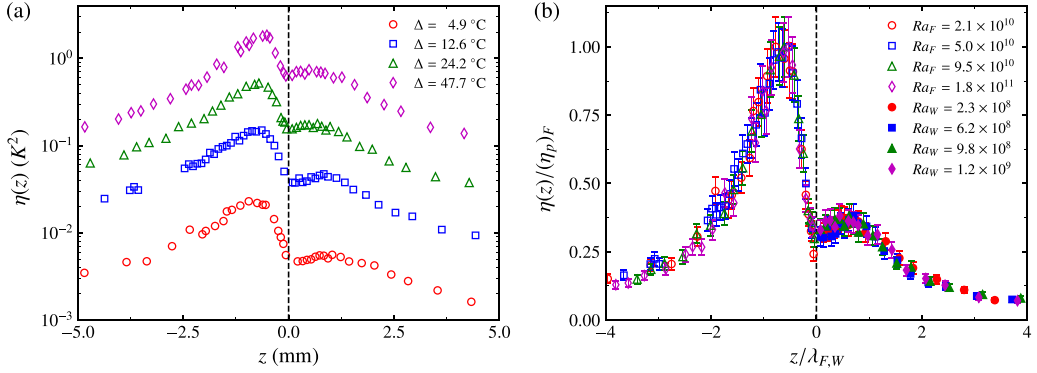


FIG. 3. (a) Measured temperature variance profiles $\eta(z)$ (colored symbols) as a function of distance z for different temperature differences Δ across the convection cell. (b) Normalized temperature variance profiles $\eta(z)/(\eta_p)_F$ as a function of the normalized distance $z/\lambda_{F,W}$ for different Rayleigh numbers. In the plot, the measured variance profiles $\eta(z)$ are normalized by their peak height $(\eta_p)_F$ in the FC770 layer. The dashed line ($z = 0$) indicates the position of the liquid interface. The error bars show the experimental uncertainties of the measurements.

a slope of -4.07 K/mm on the water side, respectively. The results shown in Fig. 2(a) indicate that a well-developed thermal BL is formed both above and below the liquid interface.

To further understand the scaling behavior of the measured mean temperature profiles, we replot the data by normalizing the mean temperature $\langle T(z, t) \rangle_t - T_0$ with the temperature difference $T_F - T_W$ between the two bulk fluids (or across the two BLs) and normalizing the distance z by the thermal BL thickness $\lambda_{F,W}$ (λ_F or λ_W) in each fluid layer. As shown in Fig. 2(b), the normalized mean temperature profiles $(\langle T(z, t) \rangle_t - T_0)/(T_F - T_W)$ as a function of the normalized distance $z/\lambda_{F,W}$ for different Rayleigh numbers Ra_F (or Ra_W) all collapse onto a single master curve. Here the BL thickness $\lambda_{F,W}$ is determined by the distance, at which the tangent of the mean-temperature profile $\langle T(z, t) \rangle_t$ near the interface intersects the bulk temperature of each fluid layer, as indicated in Fig. 2(a). The scaling results shown in Fig. 2(b) suggest that the measured mean temperature profiles obtained in different fluid layers and at different Rayleigh numbers are determined by a single mechanism.

Figure 3(a) shows the measured temperature variance profiles, $\eta(z)$, as a function of distance z for different values of Δ . Here, the temperature variance $\eta(z)$ is defined as $\eta(z) \equiv \langle [T(z, t) - \langle T(z, t) \rangle_t]^2 \rangle_t$. All of the variance profiles exhibit a bimodal shape with a distinct peak on each side of the interface. The peak height in the FC770 layer is found to be significantly larger than that in the water layer. Moreover, the temperature variance at the liquid interface is not zero but instead is a local minimum, which is a new feature very different from that at a solid surface. The large difference in the peak height between the FC770 and water layers indicates that BL fluctuations in the FC770 layer are much larger than those in the water layer.

When the temperature variance profiles $\eta(z)$ are normalized by their peak height $(\eta_p)_F$ in the FC770 layer and the distance z is normalized by the thermal BL thickness $\lambda_{F,W}$ (λ_F or λ_W) in each fluid layer, we find all the variance profiles $\eta(z)/(\eta_p)_F$ obtained in different fluid layers and at different Rayleigh numbers collapse onto a single curve, as shown in Fig. 3(b). It is found that the peak height $(\eta_p)_W$ in the water layer scales with $(\eta_p)_F$, and their ratio $(\eta_p)_W/(\eta_p)_F$ remains at a constant value of 0.38 for different Rayleigh numbers. This explains why the peak height $(\eta_p)_F$ alone is adequate to scale the measured $\eta(z)$ in both fluid layers. The normalized profile $\eta(z)/(\eta_p)_F$ in the FC770 layer peaks at the position $z_p = (0.68 \pm 0.05)\lambda_F$ below the interface, whereas the peak position of the normalized $\eta(z)/(\eta_p)_F$ in the water layer is located at the position $z_p = (0.53 \pm 0.05)\lambda_W$ above the liquid interface. These two values of z_p near the liquid interface are smaller than

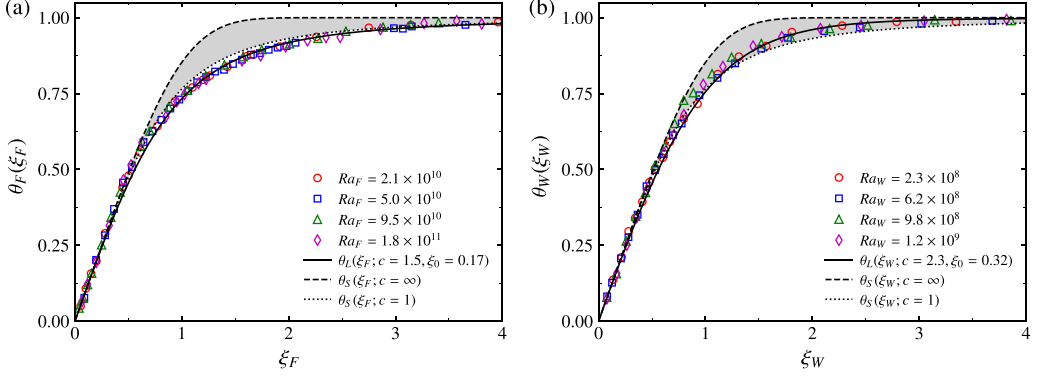


FIG. 4. (a) Normalized mean temperature profiles $\theta_F(\xi_F)$ as a function of the normalized distance ξ_F in the FC770 layer for four different values of Ra_F . The dashed and dotted lines are the calculated mean temperature profiles $\theta_S(\xi_S; c)$ near a solid surface using Eq. (4) with $c = \infty$ (PBP form) and $c = 1$, respectively. The solid line shows the calculated $\theta_L(\xi_F; c, \xi_0)$ near a liquid interface using Eq. (3) with $c = 1.5$ and $\xi_0 = 0.17$. (b) Normalized mean temperature profiles $\theta_W(\xi_W)$ as a function of the normalized distance ξ_W in the water layer for four different values of Ra_W . The dashed and dotted lines are the calculated mean temperature profiles $\theta_S(\xi_S; c)$ near a solid surface using Eq. (4) with $c = \infty$ (PBP form) and $c = 1$, respectively. The solid line shows the calculated $\theta_L(\xi_W; c, \xi_0)$ near a liquid interface using Eq. (3) with $c = 2.3$ and $\xi_0 = 0.32$.

the peak position of the normalized $\eta(z)/(\eta_p)_F$ near a solid surface, which is $0.85\lambda_S$ as reported by Wang *et al.* [5,37]. The bimodal structure of the normalized variance profiles provides further support for the establishment of two separate thermal BLs above and below the liquid interface. Similar bimodal variance profiles were also observed in a quasi-2D convection cell [25].

B. Scaling form of the normalized mean temperature and temperature variance profiles

Following the convention of defining the BL profiles near a solid surface [5,37], we now define the normalized mean temperature profile in each fluid layer separately as

$$\theta_i(\xi_i) \equiv \frac{|\langle T(\xi_i, t) \rangle_t - T_0|}{|T_i - T_0|}, \quad (7)$$

where $\xi_i = |z|/\lambda_i$ is the normalized distance away from the liquid interface and $|T_i - T_0|$ is the temperature difference across the BL. Hereafter, we use the subscript i to indicate the two fluid layers with $i = F$ for the FC770 layer and $i = W$ for the water layer. When no confusion arises (such as in the Abstract and Conclusion), the subscripts F and W will be dropped off to simplify the notation. Similarly, we define the normalized temperature variance profile in each fluid layer as

$$\Omega_i(\xi_i) \equiv \frac{\eta(\xi_i)}{(\eta_p)_i} \equiv \frac{\langle [T(\xi_i, t) - \langle T(\xi_i, t) \rangle_t]^2 \rangle_t}{(\eta_p)_i}, \quad (8)$$

where $(\eta_p)_i$ is the peak height of the measured $\eta(z)$.

Figure 4(a) shows the obtained $\theta_F(\xi_F)$ as a function of ξ_F for four different values of Ra_F . Figure 4(b) shows the obtained $\theta_W(\xi_W)$ as a function of ξ_W for four different values of Ra_W . The dashed and dotted lines in Figs. 4(a) and 4(b) are the calculated mean temperature profiles $\theta_S(\xi_S; c)$ near a solid surface using Eq. (4) with $c = \infty$ and $c = 1$, respectively. The parameter c is a measure of the level of fluctuations in the BL with $c = 1$ being the most fluctuating and $c = \infty$ being laminar (i.e., the PBP form without fluctuations). The shaded (gray-colored) region between the dashed and dotted lines indicates the region in which Eq. (4) is valid. It is seen that both the measured $\theta_F(\xi_F)$ and $\theta_W(\xi_W)$ deviate from the laminar profile (PBP form) considerably with $\theta_F(\xi_F)$ exhibiting even larger deviations outside the shaded region. This is because the FC770 layer is more turbulent with

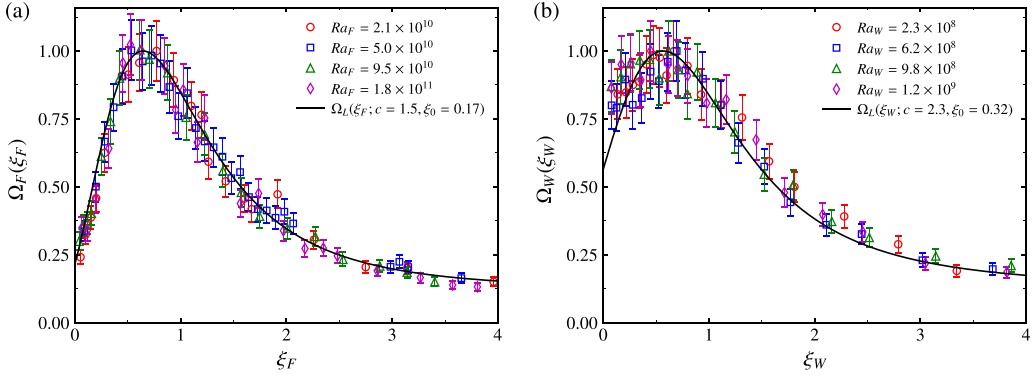


FIG. 5. (a) Normalized temperature variance profiles, $\Omega_F(\xi_F) \equiv (\eta(\xi_F)/\eta_p)_F$, as a function of the normalized distance ξ_F for four different values of Ra_F . The solid line shows the numerical solution $\Omega_L(\xi_F; c, \xi_0)$ of Eq. (5) with $c = 1.5$ and $\xi_0 = 0.17$. (b) Normalized temperature variance profiles, $\Omega_W(\xi_W) \equiv (\eta(\xi_W)/\eta_p)_W$, as a function of the normalized distance ξ_W for four different values of Ra_W . The solid line shows the numerical solution $\Omega_L(\xi_W; c, \xi_0)$ of Eq. (5) with $c = 2.3$ and $\xi_0 = 0.32$.

larger values of Ra_F and hence has more BL fluctuations. The fact that the measured $\theta_F(\xi_F)$ is outside the shaded region further demonstrates that the BL dynamics near the liquid interface are very different from those near the solid surface. Nevertheless, the measured $\theta_F(\xi_F)$ in the FC770 layer is well described by Eq. (3) with two fitting parameters, $c = 1.5$ and $\xi_0 = 0.17$ [solid line in Fig. 4(a)]. Similarly, the measured $\theta_W(\xi_W)$ in the water layer is also well described by Eq. (3) with $c = 2.3$ and $\xi_0 = 0.32$ [solid line in Fig. 4(b)].

Figure 5(a) shows the normalized temperature variance profiles, $\Omega_F(\xi_F) \equiv (\eta(\xi_F)/\eta_p)_F$, as a function of the normalized distance ξ_F for different values of Ra_F . Figure 5(b) shows the obtained $\Omega_W(\xi_W) \equiv (\eta(\xi_W)/\eta_p)_W$ as a function of the normalized distance ξ_W for different values of Ra_W . The obtained temperature variance profiles in both fluid layers can all be well described by the numerical solution $\Omega_L(\xi_L; c, \xi_0)$ of Eq. (5) for a liquid interface. The solid line in Fig. 5(a) shows the calculated $\Omega_L(\xi_F; c, \xi_0)$ using the same fitting parameters, $c = 1.5$ and $\xi_0 = 0.17$, as those used in Fig. 4(a). Similarly, the solid line in Fig. 5(b) shows the calculated $\Omega_L(\xi_W; c, \xi_0)$ using the same fitting parameters, $c = 2.3$ and $\xi_0 = 0.32$, as those used in Fig. 4(b). It is seen that in the water layer, the normalized temperature variance at the interface [$\Omega_W(z = 0)$] is larger than that in the FC770 layer, which is consistent with the observation that the peak position of the measured $\Omega_W(\xi_W)$ in the water layer is closer to the interface. This finding further demonstrates how the fitted value of the normalized thermal slip length ξ_0 in the water layer is larger than that in the FC770 layer. Compared to the measured mean temperature profiles, the temperature variance profiles are more sensitive to the changes of ξ_0 . As mentioned above, the FC770 layer has larger values of Ra_F and hence is more turbulent. Consequently, the large-scale flow in the FC770 layer will impose a stronger shear on the neighboring water layer. This strong shear effect at the liquid interface enhances the thermal slip and gives rise to a larger value of ξ_0 in the water layer. Conversely, the shear effect to the FC770 layer is relatively weaker and hence results in a smaller value of ξ_0 in the FC770 layer.

C. Spatial distribution of local temperatures in two-layer convection

When a given temperature difference, $\Delta = T_b - T_t$, is applied to the two-layer system, the temperature T_0 at the interface and hence the temperature differences, $\Delta_F = T_b - T_0$ and $\Delta_W = T_0 - T_t$, across the two fluid layers are adjusted so that a constant heat flux goes through the two-layer system, which is similar to a constant electric current going through two resistors connected in series. Because of the immiscibility and mismatch of the thermal properties between the two fluids, the temperature profile across the liquid interface forms a well-developed thermal BL on each side

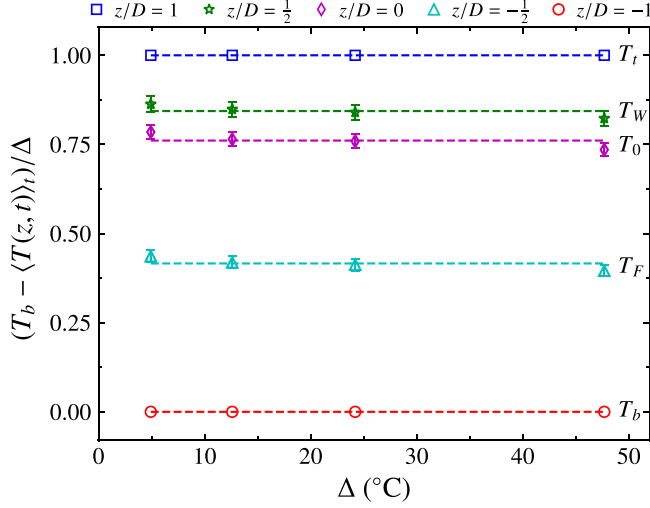


FIG. 6. Variations of the normalized local temperature, $(T_b - \langle T(z, t) \rangle_t) / \Delta$, at different locations z/D along the central axis of the convection cell for different temperature differences Δ across the convection cell. The horizontal dashed lines indicate a constant value of $(T_b - \langle T(z, t) \rangle_t) / \Delta$ for different values of Δ .

of the interface, instead of having a finite temperature jump. The two BLs are unstable, however, and emit thermal plumes on each side of the interface, giving rise to strong BL fluctuations as shown in Fig. 5. As a result, the two-layer system yields three characteristic temperatures, the two bulk fluid temperatures T_F and T_W and an interface temperature T_0 , in response to the applied temperature difference Δ across the entire convection cell.

Figure 6 shows how the normalized local temperature $(T_b - \langle T(z, t) \rangle_t) / \Delta$ changes at different locations z/D along the central axis of the convection cell for different temperature differences Δ . It is seen that the three characteristic temperatures, the bulk temperature T_F ($z/D = -0.5$) of the FC770 layer, the interface temperature T_0 ($z/D = 0$), and the bulk temperature T_W ($z/D = 0.5$) of the water layer, once normalized by the temperature difference Δ across the whole cell, all reveal a very weak dependence on Δ (slightly decrease with increasing Δ). It is seen that approximately 76% of Δ is distributed across the FC770 layer, and the other 24% of Δ is distributed across the water layer. Similarly, the temperature difference, $T_F - T_0$, across the lower BL below the interface is considerably larger than that $(T_0 - T_W)$ across the upper BL above the interface. The bulk fluid temperature in each layer is no longer an arithmetic mean of the conducting plate temperature (T_b or T_t) and interface temperature (T_0), as in the case for single-fluid convection under the Oberbeck-Boussinesq (OB) condition. Instead, both T_F and T_W show a significant shift towards the interface temperature T_0 . As will be shown in Fig. 7(b) below, this shift of the bulk fluid temperature towards T_0 is caused primarily by the broken symmetry between the BL near the bottom conducting plate with the no-slip boundary condition and the BL near the top liquid interface with a slip boundary condition.

To quantitatively describe the temperature shift of the bulk fluid in each layer, we define an asymmetry parameter χ_F in the FC770 layer as

$$\chi_F = \frac{T_F - T_0}{T_b - T_F}. \quad (9)$$

When the bulk fluid temperature is an arithmetic mean of two symmetric BLs, i.e., $T_F = (T_b + T_0)/2$, we have $\chi_F = 1$. Similarly, we define the parameter χ_W in the water layer as

$$\chi_W = \frac{T_0 - T_W}{T_W - T_t}. \quad (10)$$

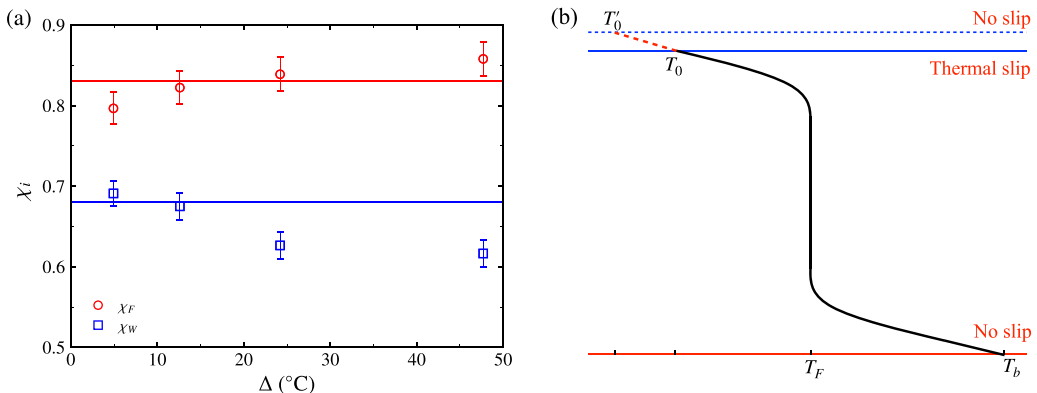


FIG. 7. (a) Measured asymmetry parameters, χ_F (red circles) and χ_W (blue squares), as a function of the temperature difference Δ across the convection cell. The red and blue solid lines are plots of Eq. (11) with $(\xi_0)_F = 0.17$ and $(\xi_0)_W = 0.32$, respectively. (b) Sketch of a typical temperature variation (black solid line) across the FC770 layer in two-layer convection. The bottom red solid line indicates the solid conducting plate with the no-slip boundary condition. The top blue solid line indicates the liquid interface with a slip boundary condition. The top blue dashed line indicates an extrapolated interface, at which the extrapolated mean temperature profile (red dotted line) becomes nonslip with a modified interface temperature T'_0 .

These two parameters have been used previously to describe the non-Oberbeck-Boussinesq (NOB) effect for single-fluid convection [42–46]. Figure 7(a) shows how the asymmetry parameters, χ_F and χ_W , change with different temperature differences Δ across the convection cell.

To further understand the asymmetric behavior of the measured χ_F and χ_W as shown in Fig. 7(a), we take the FC770 layer as an example and consider the effect of its thermal BL slip near the liquid interface. As illustrated in Fig. 7(b), the presence of the thermal BL slip at the top liquid interface causes a temperature offset, $T_0 - T'_0 \simeq (\xi_0)_F(T_b - T_F)$, at the top boundary. Here T'_0 is the modified temperature of an extrapolated interface (top blue dashed line), at which the extrapolated mean temperature profile (red dotted line) becomes nonslip. When the top and bottom boundaries are both under the no-slip boundary condition, the temperature difference across the bottom BL becomes equal to that across the top BL, i.e., $T_b - T_F = T_F - T'_0$. Therefore, the two parameters defined in Eqs. (9) and (10) become

$$\chi_i \simeq 1 - (\xi_0)_i, \quad (11)$$

where $\xi_0 = \ell_T/\lambda_S$ is the normalized slip length. From Fig. 7(b), we have $\lambda_S \simeq \lambda_L + \ell_T$ and hence $\xi_0 \simeq \ell_T/(\ell_T + \lambda_L) = (1 + \lambda_L/\ell_T)^{-1}$ [25]. The red and blue solid lines in Fig. 7(a) show the theoretical prediction of Eq. (11) for the two fluid layers, which capture the essential changes of the measured χ_F and χ_W . Small variations of the measured χ_F and χ_W with the temperature difference Δ across the convection cell are caused by other effects not considered here, such as the NOB effects in both the FC770 layer and the water layer at different Prandtl numbers Pr_W (varied in the range 4.3–7.3) [42–46].

We now consider the heat transfer across the liquid interface, which involves both the conductive $[-k(d\langle T(z, t) \rangle_i/dz)]$ and convective $(\rho C_p \langle w'T' \rangle_i)$ contributions, where C_p is the specific heat of the convecting fluid. For the local measurement of the mean temperature profile $\langle T(z, t) \rangle_i$ along the central axis of the convection cell, one also needs to consider the effect that the local heat flux may also go horizontally in parallel with the liquid interface. These complex dynamic processes at the interface make the conductive heat flux across the liquid interface nonconserved locally, namely,

$$k_F \frac{T_F - T_0}{\lambda_F} \neq k_W \frac{T_0 - T_W}{\lambda_W}. \quad (12)$$

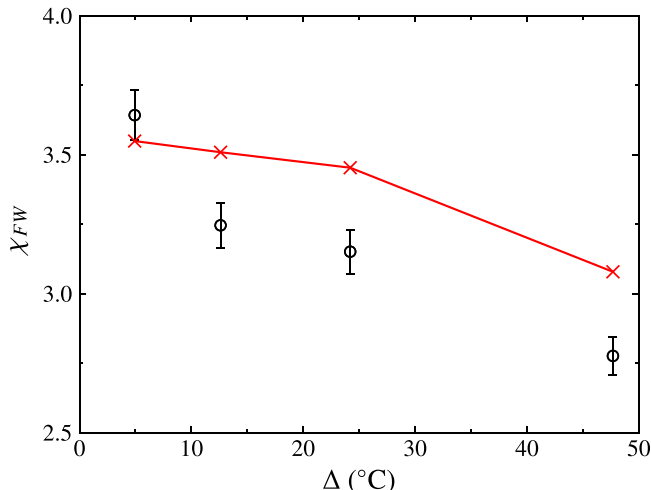


FIG. 8. Measured temperature ratio χ_{FW} (black circles) as a function of the temperature difference Δ across the convection cell. The red crosses show the calculated χ_{FW} using Eq. (15) with $\omega = 0.29$ and $\alpha = 0.14$. The red solid line is drawn to guide the eye.

The inequality in Eq. (12) can be checked with the numerical numbers given in Tables I and II. It explains why the ratio of the measured temperature gradient above the interface to that below the interface, as shown in Fig. 2(a), is not equal to the thermal conductivity ratio k_F/k_W .

In contrast, the local heat flux through the bottom and top conducting plates is conserved and we have

$$k_F \frac{T_b - T_F}{\lambda'_F} = k_W \frac{T_W - T_i}{\lambda'_W}, \quad (13)$$

where λ'_F and λ'_W denote the thermal BL thickness near the bottom and top conducting plates, respectively. Using the Grossmann-Lohse theory [47,48], we have the scaling relation between the thermal BL thickness and the local Rayleigh number and local Prandtl number

$$\lambda'_i \sim \text{Ra}_i^{-\omega} \text{Pr}_i^{-\alpha}, \quad (14)$$

where $\omega = 0.29 \pm 0.03$ and $\alpha = 0.14 \pm 0.03$ for the upright cylinder [37]. For other cell geometries, the measured values of ω and α have shown a weak dependence on the cell geometry [49–51]. By combining Eqs. (9)–(11) and Eqs. (13) and (14), we find the ratio of the temperature difference $T_b - T_0$ across the FC770 layer to the temperature difference $T_0 - T_i$ across the water layer,

$$\chi_{FW} = \frac{T_b - T_0}{T_0 - T_i} \simeq \left(\frac{2 - (\xi_0)_F}{2 - (\xi_0)_W} \right)^{\frac{1}{1+\omega}} \left(\frac{k_W}{k_F} \right)^{\frac{1}{1+\omega}} \left(\frac{\beta_W}{\beta_F} \right)^{\frac{\omega}{1+\omega}} \left(\frac{\kappa_F}{\kappa_W} \right)^{\frac{\omega+\alpha}{1+\omega}} \left(\frac{\nu_W}{\nu_F} \right)^{\frac{\omega-\alpha}{1+\omega}}. \quad (15)$$

In the above, the first factor on the right-hand side of the equation represents the influence of thermal BL slip, whereas the remaining factors account for the difference in the fluid properties of the two layers. Equation (15) is an extension of a previous result obtained by Liu *et al.* [20] for an idealized system, in which the thermal properties such as thermal expansion coefficient (β_i), thermal diffusivity (κ_i), and kinematic viscosity (ν_i) in the two fluid layers were assumed to be the same and the effect of thermal BL slip at the interface was not considered. In Eq. (15), we have included these new effects in the actual two-layer system.

Figure 8 shows the measured temperature ratio χ_{FW} as a function of the temperature difference Δ across the convection cell. The red crosses show the calculated χ_{FW} using Eq. (15) with $\omega = 0.29$ and $\alpha = 0.14$. It is seen that the calculated χ_{FW} without any adjustable parameter gives a good

estimate of the experimental results. As mentioned in Sec. II, when the temperature difference Δ is varied in the experiment, the bulk temperature T_F of the FC770 layer is kept constant (40°C) so that its fluid properties remain unchanged. The bulk temperature T_W of the water layer, however, is varied from 19.2 to 37.0°C, so that its four fluid parameters and especially the thermal expansion coefficient (β_W) and kinematic viscosity (ν_W) change considerably. As a result, the obtained values of χ_{FW} decrease modestly with increasing Δ . Figure 8 thus confirms that Eq. (15) provides a quantitative relation that can be used to determine the interface temperature T_0 for a given Δ .

IV. CONCLUSION

In this work, we carried out a systematic experimental study of turbulent two-layer convection in an upright cylinder. The two-layer system consists of two stacked layers of immiscible fluids, FC770 and water, in which a stable liquid interface is formed even when each fluid layer is under turbulent thermal convection. The normalized mean temperature profile $\theta(z)$ and temperature variance profile $\Omega(z)$, as a function of distance z away from the interface, were measured along the central vertical axis of the convection cell with varying temperature difference Δ across the cell. In the experiments with varying Δ , the bulk temperature T_F of the FC770 layer was kept constant (40°C) whereas the bulk temperature T_W of the water layer was varied from 19.2 to 37.0°C. Correspondingly, the local Rayleigh number of each liquid layer was varied, respectively, in the ranges of $2.1 \times 10^{10} \lesssim \text{Ra}_F \lesssim 1.8 \times 10^{11}$ and $2.3 \times 10^8 \lesssim \text{Ra}_W \lesssim 1.2 \times 10^9$.

From the measured mean temperature and temperature variance profiles, we find a unique twin-boundary-layer structure across the liquid interface with one of the twin BLs residing on each side of the interface. The measured $\theta(z)$ and $\Omega(z)$ in each fluid layer with different local Rayleigh numbers are found to have the scaling forms $\theta(z/\lambda)$ and $\Omega(z/\lambda)$, respectively. The functional form of the obtained $\theta(z/\lambda)$ and $\Omega(z/\lambda)$ near the liquid interface is well described by the BL equations for a solid conducting plate, so long as a thermal slip length ℓ_T [or its normalized value $\xi_0 = (1 + \lambda/\ell_T)^{-1}$] is introduced to account for the convective heat flux passing through the liquid interface. While the obtained $\theta(z/\lambda)$ and $\Omega(z/\lambda)$ for the twin BLs share the same scaling forms, as described by Huang *et al.* [25], they nevertheless have different BL thickness λ and slip length ℓ_T (or ξ_0) in the two fluid layers. This work represents a further extension of the recent experiment by Huang *et al.* [25] in a quasi-2D convection cell. Here we investigate the flow properties of both the fluid layers above and below the liquid interface simultaneously. Interestingly, even in the more complex three-dimensional system with a larger number of flow modes, thermal slip is observed in both the fluid layers with the water layer having a lower Rayleigh number and exhibiting a larger thermal slip length ℓ_T . The larger value of ℓ_T results from a stronger shear effect to the liquid interface imposed by the FC770 layer, which has a larger value of Ra_F and hence is more turbulent.

Furthermore, three characteristic temperatures are found as response parameters in the two-layer convection, namely, the temperature T_0 of the interface, the bulk temperature T_F of the FC770 layer, and the bulk temperature T_W of the water layer. The three characteristic temperatures, once normalized by the temperature difference Δ across the whole cell, all reveal a very weak dependence on Δ (slightly decrease with increasing Δ). Compared with turbulent convection in a single fluid layer under symmetric boundary conditions, the two bulk fluid temperatures, T_F and T_W , show a significant shift towards the interface temperature T_0 , primarily due to the broken symmetry between the BL near the solid conducting plate and that near the liquid interface. This temperature shift is quantitatively described by two asymmetry parameters, χ_F and χ_W , which are directly linked to the normalized slip length ξ_0 , as shown in Eq. (11). By combining the scaling result of heat transport across the entire cell and the two asymmetry parameters χ_F and χ_W , we obtain a quantitative relation that links the interface temperature T_0 to ξ_0 and other fluid properties, as shown in Eq. (15). The theoretical results are found to be in good agreement with the experimental values.

In this work, the thickness ratio of the two fluid layers is kept at unity. The interfacial tension γ' between the two fluids also remains unchanged. How the thickness ratio of the two fluid layers affects the thermal slip length in each layer and the heat transport across the whole convection cell

is an interesting subject for future study [20]. According to Eq. (15), the changes in the thermal slip length will, in turn, affect the distribution of the temperature differences across the two fluid layers. The effect of the interfacial tension γ' on the thermal slip length is also an interesting subject for future study. The interface between the two fluid layers may become unstable when the control parameters (Ra_i , We) are in a critical regime [19]. The current study represents the first step toward these directions.

ACKNOWLEDGMENTS

This work was supported in part by the Hong Kong RGC under Grant No. N_HKUST604/19 (P.T.) and by the Center for Ocean Research in Hong Kong and Macau (CORE) jointly established by the Laoshan Laboratory and HKUST. X.H. acknowledges the support of the National Natural Science Foundation of China (Grant No. 12372216), the Science, Technology and Innovation Commission of Shenzhen Municipality (Grant No. GXWD20220818113020001), and the Fundamental Research Funds for the Central Universities (Grant No. HIT.OCEF.2023046).

-
- [1] R. Krishnamurti and L. N. Howard, Large-scale flow generation in turbulent convection, *Proc. Natl. Acad. Sci. USA* **78**, 1981 (1981).
 - [2] G. Zocchi, E. Moses, and A. Libchaber, Coherent structures in turbulent convection, an experimental study, *Phys. A: Stat. Mech.* **166**, 387 (1990).
 - [3] L. P. Kadanoff, Turbulent heat flow: Structures and scaling, *Phys. Today* **54**(8), 34 (2001).
 - [4] O. Shishkina, S. Horn, S. Wagner, and E. S. Ching, Thermal boundary layer equation for turbulent Rayleigh–Bénard convection, *Phys. Rev. Lett.* **114**, 114302 (2015).
 - [5] Y. Wang, X. He, and P. Tong, Boundary layer fluctuations and their effects on mean and variance temperature profiles in turbulent Rayleigh–Bénard convection, *Phys. Rev. Fluids* **1**, 082301(R) (2016).
 - [6] Y. Wang, P.-Y. Lai, H. Song, and P. Tong, Mechanism of large-scale flow reversals in turbulent thermal convection, *Sci. Adv.* **4**, eaat7480 (2018).
 - [7] Y.-B. Du and P. Tong, Turbulent thermal convection in a cell with ordered rough boundaries, *J. Fluid Mech.* **407**, 57 (2000).
 - [8] X.-L. Qiu and P. Tong, Large-scale velocity structures in turbulent thermal convection, *Phys. Rev. E* **64**, 036304 (2001).
 - [9] H.-D. Xi, S. Lam, and K.-Q. Xia, From laminar plumes to organized flows: The onset of large-scale circulation in turbulent thermal convection, *J. Fluid Mech.* **503**, 47 (1999).
 - [10] C. Sun, K. Q. Xia, and P. Tong, Three-dimensional flow structures and dynamics of turbulent thermal convection in a cylindrical cell, *Phys. Rev. E* **72**, 026302 (2005).
 - [11] G. Ahlers, S. Grossmann, and D. Lohse, Heat transfer and large scale dynamics in turbulent Rayleigh–Bénard convection, *Rev. Mod. Phys.* **81**, 503 (2009).
 - [12] F. Chillà and J. Schumacher, New perspectives in turbulent Rayleigh–Bénard convection, *Eur. Phys. J. E* **35**, 1 (2012).
 - [13] S. Rasenat, F. H. Busse, and I. Rehberg, A theoretical and experimental study of double-layer convection, *J. Fluid Mech.* **199**, 519 (1989).
 - [14] F. H. Busse and M. Petry, Homologous onset of double layer convection, *Phys. Rev. E* **80**, 046316 (2009).
 - [15] A. Juel, J. M. Burgess, W. D. McCormick, J. B. Swift, and H. L. Swinney, Surface tension-driven convection patterns in two liquid layers, *Physica D: Nonlinear Phenom.* **143**, 169 (2000).
 - [16] C. D. Andereck, P. W. Colovas, M. M. Degen, and Y. Y. Renardy, Instabilities in two-layer Rayleigh–Bénard convection: Overview and outlook, *Int. J. Eng. Sci.* **36**, 1451 (1998).
 - [17] A. Nepomnyashchy, J. C. Legros, and I. Simanovskii, *Interfacial Convection in Multilayer Systems* (Springer, New York, NY, 2006).

- [18] Y.-C. Xie and K.-Q. Xia, Dynamics and flow coupling in two-layer turbulent thermal convection, *J. Fluid Mech.* **728**, R1 (2013).
- [19] H.-R. Liu, K. L. Chong, Q. Wang, C. S. Ng, R. Verzicco, and D. Lohse, Two-layer thermally driven turbulence: Mechanisms for interface breakup, *J. Fluid Mech.* **913**, A9 (2021).
- [20] H.-R. Liu, K. L. Chong, R. Yang, R. Verzicco, and D. Lohse, Heat transfer in turbulent Rayleigh–Bénard convection through two immiscible fluid layers, *J. Fluid Mech.* **938**, A31 (2022).
- [21] M. Yoshida and Y. Hamano, Numerical studies on the dynamics of two-layer Rayleigh–Bénard convection with an infinite Prandtl number and large viscosity contrasts, *Phys. Fluids* **28**, 116601 (2016).
- [22] M. Wang, X.-Y. Chen, W. Wang, and P. Wei, Heat transport and flow structure in thermal convection with two liquid layers, *J. Fluid Mech.* **978**, A4 (2023).
- [23] H. Song, E. Villermaux, and P. Tong, Coherent oscillations of turbulent Rayleigh–Bénard convection in a thin vertical disk, *Phys. Rev. Lett.* **106**, 184504 (2011).
- [24] Y. Wang, X. He, and P. Tong, Turbulent temperature fluctuations in a closed Rayleigh–Bénard convection cell, *J. Fluid Mech.* **874**, 263 (2019).
- [25] H. Huang, W. Xu, Y. Wang, X. Wang, X. He, and P. Tong, Fluctuation-induced slip of thermal boundary layers at a stable liquid–liquid interface, *J. Fluid Mech.* **951**, A10 (2022).
- [26] J. D. Neelin, M. Latif, and F. Jin, Dynamics of coupled ocean–atmosphere models: The tropical problem, *Annu. Rev. Fluid Mech.* **26**, 617 (1994).
- [27] P. Olson, P. G. Silver, and R. W. Carlson, The large-scale structure of convection in the earth’s mantle, *Nature (London)* **344**, 209 (1990).
- [28] G. F. Davies and M. A. Richards, Mantle convection, *J. Geol.* **100**, 151 (1992).
- [29] J. Szekely, *Fluid Flow Phenomena in Metals Processing* (Elsevier, Amsterdam, 2012)
- [30] K. Holmberg, *Handbook of Applied Surface and Colloid Chemistry* (Wiley, Chichester, UK/New York, NY, 2002).
- [31] J. B. Grotberg and O. E. Jensen, Biofluid mechanics in flexible tubes, *Annu. Rev. Fluid Mech.* **36**, 121 (2004).
- [32] L. D. Landau and E. M. Lifshitz, *Fluid Mechanics* (Pergamon Press, Oxford, UK, 1987).
- [33] E. Brown and G. Ahlers, Azimuthal asymmetries of the large-scale circulation in turbulent Rayleigh–Bénard convection, *Phys. Fluids* **20**, 105105 (2008).
- [34] E. Brown and G. Ahlers, The origin of oscillations of the large-scale circulation of turbulent Rayleigh–Bénard convection, *J. Fluid Mech.* **638**, 383 (2009).
- [35] H.-D. Xi, S.-Q. Zhou, Q. Zhou, T.-S. Chan, and K.-Q. Xia, Origin of the temperature oscillation in turbulent thermal convection, *Phys. Rev. Lett.* **102**, 044503 (2009).
- [36] D. Ji and E. Brown, Low-dimensional model of the large-scale circulation of turbulent Rayleigh–Bénard convection in a cubic container, *Phys. Rev. Fluids* **5**, 064606 (2020).
- [37] Y. Wang, W. Xu, X. He, H. Yik, X. Wang, J. Schumacher, and P. Tong, Boundary layer fluctuations in turbulent Rayleigh–Bénard convection, *J. Fluid Mech.* **840**, 408 (2018).
- [38] X. He and P. Tong, Measurements of the thermal dissipation field in turbulent Rayleigh–Bénard convection, *Phys. Rev. E* **79**, 026306 (2009).
- [39] Y. Wang, Y. Wei, P. Tong, and X. He, Collective effect of thermal plumes on temperature fluctuations in a closed Rayleigh–Bénard convection cell, *J. Fluid Mech.* **934**, A13 (2022).
- [40] D. R. Lide, *CRC Handbook of Chemistry and Physics*, Vol. 85 (CRC Press, Boca Raton, FL, 2004).
- [41] L. Méthivier, R. Braun, F. Chillà, and J. Salort, Turbulent transition in Rayleigh–Bénard convection with fluorocarbon, *Europhys. Lett.* **136**, 10003 (2021).
- [42] J. Zhang, S. Childress, and A. Libchaber, Non-Boussinesq effect: Thermal convection with broken symmetry, *Phys. Fluids* **9**, 1034 (1997).
- [43] G. Ahlers, E. Brown, F. F. Araujo, D. Funfschilling, S. Grossmann, and D. Lohse, Non-Oberbeck–Boussinesq effects in strongly turbulent Rayleigh–Bénard convection, *J. Fluid Mech.* **569**, 409 (2006).
- [44] G. Ahlers, F. Fontenele Araujo, D. Funfschilling, S. Grossmann, and D. Lohse, Non-Oberbeck–Boussinesq effects in gaseous Rayleigh–Bénard convection, *Phys. Rev. Lett.* **98**, 054501 (2007).

- [45] G. Ahlers, E. Calzavarini, F. Fontenele Araujo, D. Funfschilling, S. Grossmann, D. Lohse, and K. Sugiyama, Non–Oberbeck–Boussinesq effects in turbulent thermal convection in ethane close to the critical point, [Phys. Rev. E](#) **77**, 046302 (2008).
- [46] S. Weiss, X. He, G. Ahlers, E. Bodenschatz, and O. Shishkina, Bulk temperature and heat transport in turbulent Rayleigh–Bénard convection of fluids with temperature–dependent properties, [J. Fluid Mech.](#) **851**, 374 (2018).
- [47] S. Grossmann, The onset of shear flow turbulence, [Rev. Mod. Phys.](#) **72**, 603 (2000).
- [48] S. Grossmann and D. Lohse, Scaling in thermal convection: A unifying view, [J. Fluid Mech.](#) **407**, 27 (2000).
- [49] H. Song and P. Tong, Scaling laws in turbulent Rayleigh–Bénard convection under different geometry, [Europhys. Lett.](#) **90**, 44001 (2010).
- [50] J. Bailon-cuba, M. S. Emran, and J. Schumacher, Aspect ratio dependence of heat transfer and large–scale flow in turbulent convection, [J. Fluid Mech.](#) **655**, 152 (2010).
- [51] G. Ahlers, E. Bodenschatz, R. Hartmann, X. He, D. Lohse, P. Reiter, R. J. Stevens, R. Verzicco, M. Wedi, S. Weiss, X. Zhang, L. Zvirner, and O. Shishkina, Aspect ratio dependence of heat transfer in a cylindrical Rayleigh–Bénard cell, [Phys. Rev. Lett.](#) **128**, 084501 (2022).